Journal of Power Sources 212 (2012) 161–168

Contents lists available at SciVerse ScienceDirect

Journal of Power Sources

journal homepage: www.elsevier.com/locate/jpowsour

# Characterisation and optimisation of the cathode/electrolyte couple for SOFC LSCF/BIT07

Marika Letilly, Olivier Joubert, Annie Le Gal La Salle*

*Institut des Matériaux Jean Rouxel (IMN), CNRS-Université de Nantes, 2 rue de la Houssinière, BP 32229, 44322 Nantes, France*

ARTICLE INFO

*Article history:*
Received 9 January 2012
Received in revised form
9 March 2012
Accepted 15 March 2012
Available online 10 April 2012

*Keywords:*
BIT07
LSCF
SOFC
EIS
Optimisation
Ageing

ABSTRACT

$BaIn_{0.3}Ti_{0.7}O_{2.85}$ (BIT07) is a new electrolyte material for solid oxide fuel cells (SOFC). Its use with the cathode material $La_{0.58}Sr_{0.4}Co_{0.2}Fe_{0.8}O_{3-\delta}$ (LSCF) is advantageous due to their reaction (above 1000 °C) that leads to the formation of perovskite compounds called BLSITCFx ($Ba_xLa_{0.58(1-x)}Sr_{0.4(1-x)}In_{0.3x}Ti_{0.7x}Co_{0.2(1-x)}Fe_{0.8(1-x)}O_{3-\delta}$, with $0 \leq x \leq 1$) at the cathode/electrolyte interface. In this study, the influence of the cathode microstructure on its performance has been investigated, by varying the cathode parameters. An area specific resistance (ASR) value of 0.07 Ω cm$^2$ at 700 °C has been reached and more generally the cathodes exhibit good performance (below 0.2 Ω cm$^2$) for a large range of thermal treatments, cathode grain sizes and thicknesses. An ageing study realised at 700 °C for 320 h showed an ageing rate of 0.125% h$^{-1}$.



## 1. Introduction

SOFC are all-solid devices converting the chemical energy of gaseous fuels, such as hydrogen or natural gas, into electricity via electrochemical processes and presenting advantages such as high energy conversion efficiency, low greenhouse gas emission, or flexibility of fuels [1]. At high operating temperatures (800–1000 °C), the fuel cell materials degradation is accelerated and thus lowering the working temperature of SOFC is necessary [2]. However, the SOFC performance decreases strongly when the operating temperature is lower, due to the increase of both the electrode polarisation and the electrolyte resistance. To develop a SOFC with high power output at intermediate temperatures (600–800 °C), it is essential to reduce both the polarisation and resistance losses of the cell.

Perovskite oxides, particularly mixed ionic and electronic conductors (MIECs), are the most commonly used cathode materials for those intermediate-temperature solid oxide fuel cells (IT-SOFCs), and among them LSCF ($La_{0.58}Sr_{0.4}Co_{0.2}Fe_{0.8}O_{3-\delta}$) is widely used [3]. Nevertheless, its use with the electrolyte material YSZ is limited by the formation of an insulating layer of $SrZrO_3$ [4], and the addition of an intermediate layer is often necessary [5,6]. With other electrolytes, such as Gd- or Sm doped $CeO_2$ [7,8] or LSGM ($La_{0.9}Sr_{0.1}Ga_{0.8}Mg_{0.2}O_{3-\delta}$) [9], the use of composite electrolyte-LSCF, instead of pure LSCF, is often recommended to reduce the reactivity between the cathode and electrolyte materials. Even if the employment of pure LSCF without interlayer association has been already reported, the sintering process must be performed at moderate temperatures in order to obtain a good cohesion between electrolyte and LSCF without generating an insulating layer [10]. The study of the cell preparation is necessary not only to optimise the interface cathode/electrolyte, but also the performance of the cathode itself [11,12]. Therefore it appears that the operation of YSZ-based electrolytes with LSCF requires numerous optimisation studies and that the research for new LSCF/electrolyte couples is still necessary [13].

Research of new reliable ion-conducting oxides to replace YSZ has generated many studies. Ceria based materials [14,15] and $Ba_2In_2O_5$ substituted compounds such as $BaIn_{0.3}Ti_{0.7}O_{2.85}$ (BIT07) [16] are examples of this intense research. Nevertheless, the application of these good ionic conductors as electrolyte materials for IT-SOFCs requires also a good compatibility with the cathode materials in terms of quality of the interface even after long-term cycle life. In a previous study, the authors have validated the use of BIT07 electrolyte with usual cathode materials ($La_{0.7}Sr_{0.3}MnO_{3-\delta}$, LSCF and $Nd_2NiO_{4+\delta}$) [17]. Without any optimisation, an ASR value

* Corresponding author. Tel.: +33 240373913; fax: +33 240373995.
*E-mail address:* annie.legal@cnrs-imn.fr (A. Le Gal La Salle).

0378-7753/$ – see front matter © 2012 Elsevier B.V. All rights reserved.
doi:10.1016/j.jpowsour.2012.03.042

down to 0.10 Ω cm$^2$ at 700 °C was observed for LSCF. In spite of the discrepancy between the TECs of the cathode and electrolyte materials ($12.2 \times 10^{-6}$ K$^{-1}$ for BIT07 instead of $24.5 \times 10^{-6}$ K$^{-1}$ for LSCF at 700 °C), a rather good adhesion was observed at the BIT07/LSCF interface [17].

In another study, the authors have shown that BIT07 and LSCF can react above 1000 °C, to form of a perovskite type phase [18]. The product of the reaction between $x$ mol of BIT07 and $(1-x)$ mol of LSCF is a MIEC with the chemical formula $Ba_xLa_{0.58(1-x)}Sr_{0.4(1-x)}In_{0.3x}Ti_{0.7x}Co_{0.2(1-x)}Fe_{0.8(1-x)}O_{3-\delta}$ (with $0 \leq x \leq 1$), called BLSITCFx. Consequently, during the sintering step of the cathode layer, which is realised above 1000 °C, the formation of those BLSITCFx phases can happen at the cathode/electrolyte interface. It has been seen that the phases BLSITCFx exhibit both electrochemical and mechanical properties that vary continuously between BIT07 and LSCF. Thus, at the interface, the formation of an accommodating layer, enhancing adhesion between cathode and electrolyte and explaining the LSCF/BIT07 mechanical cohesion is expected. Moreover, the products of reaction between LSCF and BIT07 (BLSITCFx) are not insulating phases, on the contrary to what happens between LSCF and YSZ ($SrZrO_3$ and $La_2Zr_2O_7$). This self-induced interface, formed during the cathode sintering treatment, could also lead to a noticeable reduction of the total cost of the cell because it does not require additional synthesis, design or firing step.

In an IT-SOFC, the cathode induces large performance losses. Therefore, the cathode microstructure has to be well controlled as it governs several phenomena and also their kinetics: (i) the diffusion of gas ($O_2$), (ii) the adsorption of the gas on the grain surface, (iii) the conduction of electrons, (iv) the incorporation of ions ($O^{2-}$) into the bulk, (v) the conduction of ions $O^{2-}$, etc… [19] In order to study the influence of the microstructure on both the cathode polarisation resistance and the cohesion of the electrolyte/cathode interface, several parameters have been investigated: (i) the cathode thickness, (ii) the sintering duration, (iii) the sintering temperature and (iv) the cathode grain size [20]. Optimisation of these parameters has been done by comparing the ASR (at 700 °C) of the corresponding half cells.

An ageing study has also been carried out: the electrochemical performance of a cathode/electrolyte/cathode assembly has been recorded at 700 °C under air during 320 h.

## 2. Experimental

### 2.1. Powders

BIT07 was synthesised as detailed in Ref. [16]: its constituents, high purity barium carbonate (Alfa Aesar), indium oxide (Alfa Aesar) and titanium dioxide (Merck), in stoichiometric ratio, were mixed in mortar and pestle using alcohol. The mixture was first heated at 1200 °C for 24 h, then ground and compacted into a pellet of 40 mm diameter. This compact was then heated at 1350 °C for 24 h, ground and passed through mesh 100. The as-synthesised powder exhibits a $d_{90}$ of 14 μm, thus it has been ball-milled in 45 ml silicon nitride pot with 15 silicon nitride balls in ethanol at 500 rpm using FRITSCH P7 planetary micro mill for 4 h, in order to decrease the $d_{90}$ to 6 μm [21]. Electrolyte substrates have been realised by pressing this ball-milled powder into 13 mm pellets. They have then been fired at 1400 °C for 24 h [22] in order to obtain dense substrate (thickness ≈ 0.4 mm and diameter: 10 mm), with a compacity above 92%.

LSCF powder, with a grain size exhibiting a $d_{90}$ of 50 μm, was provided by Marion Technologies. This powder has also been ball-milled in 45 ml silicon nitride pot with 15 silicon nitride balls in ethanol at 500 rpm using FRITSCH P7 planetary micro mill for 4 or 15 h in order to reduce the grain size [23]. The powders characteristics have been determined: specific surface areas have been measured by BET measurement (Micromeritics ASAP 2010) and the grain sizes have been obtained by laser size grading (Coulter LS 230).

**Table 1**
Design of experiments parameters, notations and chosen values.

| Parameter | Notation (unit) | Values |
|---|---|---|
| Firing temperature | $T$ (°C) | 1000–1050–1100–1150 |
| Firing duration | $t$ (h) | 2–4–6 |
| Nb of deposited layers | $n$ | 2–4–6 |
| Ball-milling duration | $b$ (h) | 4–15 |

### 2.2. Preparation of symmetrical LSCF/BIT07/LSCF cells

Symmetrical cells cathode/electrolyte/cathode have been realised by screen-printing (using a DEK 245 screen printer) the LSCF powder on a dense electrolyte pellet. An ink was firstly prepared by mixing 60 wt.% of LSCF with 40 wt.% of a mixture (95 wt.% terpineol/5 wt.% ethyl cellulose). The ink is deposited through a circular (diameter: 8 mm) mask hole. The thickness of the deposit is varied by doing several successive ink deposits, with intermediate heatings at 120 °C. When the desired thickness is obtained, the pellet is heated at 120 °C for 15 min before doing the same deposits on the other side of the pellet. For these symmetrical cells a two step sintering treatment has been realised. The first step was carried out at a relatively slow rate of 50 K h$^{-1}$ up to 600 °C in order to remove slowly the organic compounds (terpineol–ethyl cellulose) without causing any damage to the deposit. The second step was realised at a rate of 100 K h$^{-1}$ up to the sintering temperature ($T$). At this temperature, a dwell time ($t$) was applied before cooling down to room temperature at 100 K h$^{-1}$. The influence of the number of deposited layers ($n$) and of the thermal treatment ($T$/°C and $t$/h) on the cathode performance will be discussed later.

### 2.3. Design of experiments

In order to study the influence of the microstructure on both the cathode polarisation resistance and the cohesion of the electrolyte/cathode interface, several parameters have been investigated. Table 1 gathers the design parameters that have been explored: the firing temperature, the firing duration, the number of layers deposited by screen-printing and the ball-milling duration of the LSCF powder (i.e. the LSCF grain size).

### 2.4. Mechanical and chemical characterisations of the cathode/electrolyte assembly

The cathode/electrolyte assembly has been observed by Scanning Electron Microscopy (SEM) using a JEOL 7600. The cathode/electrolyte interface has been analysed by Energy Dispersive X-Ray Spectrometry (EDXS) using a Bruker Quantax-EDS. Analyses were recorded at 15 kV for the elements La, Sr, Co and Fe for LSCF and Ba and In for BIT07.

**Table 2**
Specific surface areas and grain sizes of the LSCF powders obtained for the different ball-milling durations.

| Ball-milling duration (h) | Specific surface area (m$^2$ g$^{-1}$) | $d_{10}$ (μm) | $d_{50}$ (μm) | $d_{90}$ (μm) |
|---|---|---|---|---|
| 0 | 4.28 ± 0.14 | 5.37 | 29.21 | 50.39 |
| 4 | 6.17 ± 0.08 | 0.69 | 1.99 | 5.03 |
| 15 | 13.55 ± 0.10 | 0.45 | 0.65 | 1.98 |

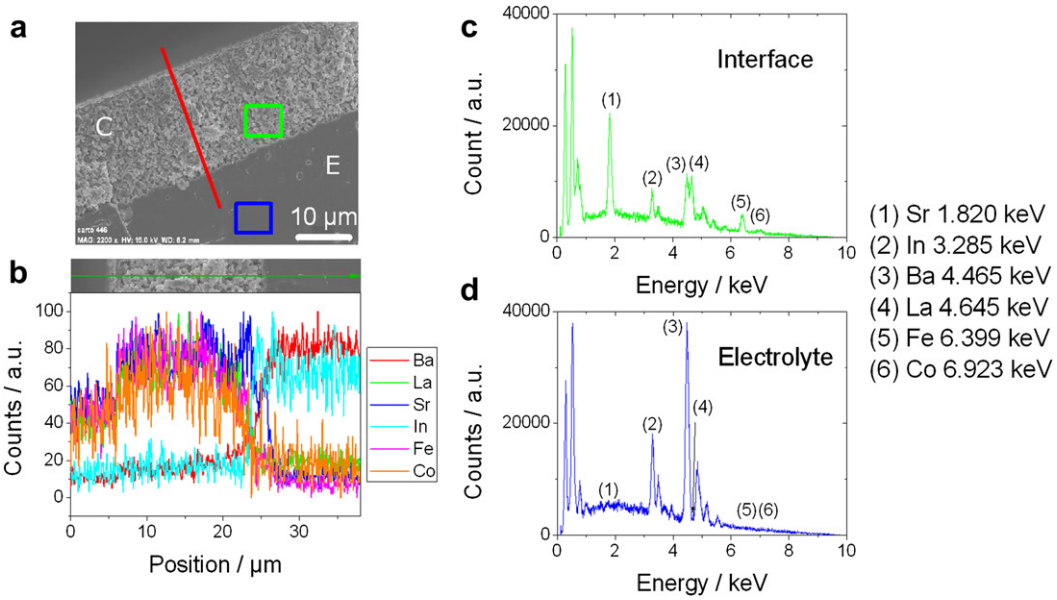


**Fig. 1.** Mechanical and chemical characterisations of an LSCF/BIT07 assembly: (a) SEM image of the fracture surface of the cathode/electrolyte assembly, (b) line concentration of Ba, La, Sr, In, Fe and Co elements along the red line depicted in (a), (c) EDXS spectrum recorded in the cathode, near the cathode/electrolyte interface (green area in (a)) and (d) EDXS spectrum recorded in the electrolyte (blue area in (a)). (For interpretation of the references to colour in this figure legend, the reader is referred to the web version of this article.)

The element Ti, present in BIT07, has not been analyse because it exhibits overlapping peaks with barium (i.e. $Ba_{(L\alpha1)}$ and $Ti_{(K\alpha1)}$ around 4.5 keV and $Ba_{(L\beta1)}$ and $Ti_{(K\beta1)}$ around 4.9 keV). The only Ti peak, that does not overlap a Ba one is the $Ti_{(L\alpha1)}$, it is encountered at 0.452 keV. But we cannot use this peak either as it exhibits a very low intensity and it overlaps the $C_{(K\alpha1)}$ and $O_{(K\alpha1)}$ peaks (encountered at 0.282 and 0.523 keV, respectively). Because of the lack of information concerning the titanium, the chemical composition of the cathode/electrolyte interface will not be given.

### 2.5. Electrochemical characterisation of the symmetrical cells

The LSCF/BIT07/LSCF symmetrical cells, contacted by gold meshes (Goodfellow, AU008710, nominal aperture: 250 µm, wire diameter: 60 µm), have been tested by electrochemical impedance spectroscopy (EIS) under air at 700 °C. Spectrum has been recorded at Udc = 0 V, with a signal amplitude of 100 mV (it has been checked that the amplitude of the perturbation signal is small enough to meet the linearity requirement of the transfer function [24,25]) and with 84 points scattered in a frequency range from 2 MHz to 0.01 Hz, with a frequency response analyser Solartron 1260. The EIS data were analysed using ZView2-Software [26].

## 3. Results and discussion

### 3.1. Powders

Table 2 gathers the characteristics of the LSCF powders obtained after the different ball-milling treatments including the specific surface areas determined by BET measurements and the grain sizes measured by laser size grading.

The two ball-milling durations that have been chosen allow to obtain powders significantly different and thus to study a wide range of cathode microstructures.

### 3.2. Mechanical and chemical characterisations of the cathode/electrolyte assembly

Fig. 1 presents the mechanical and chemical characterisations of a cathode/electrolyte assembly, the cathode is composed of LSCF powder ball-milled for 15 h and the assembly has been sintered 6 h at 1050 °C.

Fig. 1(a) attests that the cathode/electrolyte assembly exhibits a good mechanical cohesion, no delamination is observed at the interface. On Fig. 1(b), a variation of composition is observed over an area of approximately 5 µm around the cathode/electrolyte

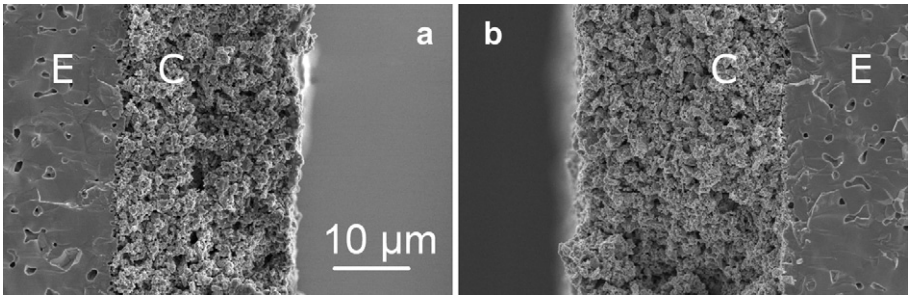


**Fig. 2.** SEM images of the fracture surface of the cathode/electrolyte assembly. The two samples are made of 6 screen-printing layers and have been sintered at 1000 °C for: (a) 6 and (b) 2 h.

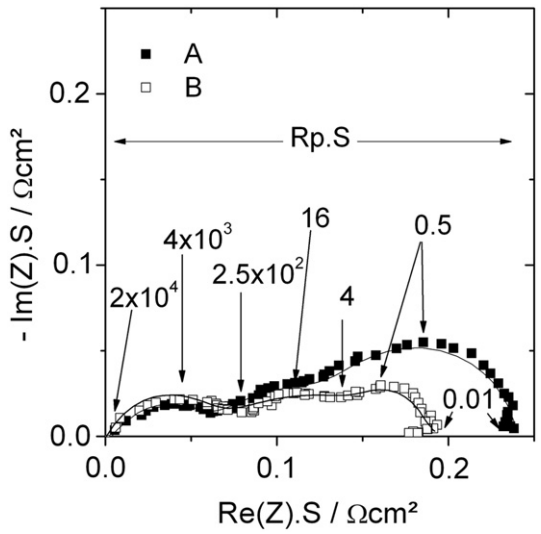


**Fig. 3.** Nyquist diagrams recorded at 700 °C for the samples A (■) and B (□). Frequencies are indicated in Hz. The lines correspond to the diagrams calculated with values gathered in Table 3.

interface. It has been demonstrated that BIT07 and LSCF start to react together at a temperature of around 1000 °C [18]. Thus this composition variation (apart from the titanium, not measured, see Section 2.4) seems to be in agreement with the formation of an accommodating layer based on both BIT07 and LSCF (i.e. BLSITCFx phases). The EDXS spectrum recorded in the cathode near the cathode/electrolyte interface (Fig. 1(c)) confirms this observation: all the elements of both BIT07 and LSCF are present. As a reference, the EDXS spectrum recorded in the electrolyte agrees with the composition of BIT07 (Fig. 1(d)).

### 3.3. Impedance measurement's validity, precision and exploitation

In the first part of the study, the grain size of the LSCF powder has been fixed by using powder ball-milled 4 h.

#### 3.3.1. Influence of the parameters on the cathode thickness

By varying the different parameters ($T$, $t$ and $n$), it is possible to vary the cathode thickness, which is directly linked to the number of layers deposited by screen-printing but also to the thermal treatment applied. Indeed, for the same number of deposited layers, the higher the thermal treatment temperature or the longer its duration, the thinner the cathode becomes. Fig. 2 presents the SEM images of two samples made with 6 screen-printing layers and heat-treated at 1000 °C. The thicknesses of the cathodes are of 23.5 μm and 31.5 μm for sintering durations of 6 and 2 h, respectively.

In the following parts, the influence of the thickness will be investigated by keeping in mind that this parameter depends on the three others: number of layers, sintering temperature and sintering duration.

**Table 3**
Comparison of resistance and capacity values determined from impedance diagrams 3A and 3B.

| Sample | $R_{MF}S$ ($\Omega\,cm^2$) | $C_{MF}/S$ ($F\,cm^{-2}$) | $R_{LF}S$ ($\Omega\,cm^2$) | $C_{LF}/S$ ($F\,cm^{-2}$) | $R_{VLF}S$ ($\Omega\,cm^2$) | $C_{VLF}/S$ ($F\,cm^{-2}$) |
|---|---|---|---|---|---|---|
| A | 0.11 | $2\times10^{-4}$ | 0.06 | $2\times10^{-1}$ | 0.06 | 4 |
| B | 0.10 | $2\times10^{-4}$ | 0.07 | $2\times10^{-1}$ | 0.02 | 5 |

#### 3.3.2. Reproducibility of the design method and accuracy of the impedance measurement

Two samples, named A and B, have been realised to check the reproducibility of both the design of the electrode by screen-printing and its electrochemical characterisation. They are both made of 4 layers and have been sintered at 1100 °C for 4 h. The two samples A and B exhibit thicknesses of 17 and 18 μm, respectively and the same mean pore size has been observed for those two sample prepared identically. This experiment attests the reproducibility of the design method since the same thickness and microstructure are obtained for the two samples.

Fig. 3 presents the Nyquist diagrams recorded at 700 °C for the two samples. The diagrams are mainly composed of three depressed semi-circles and can be modelled by the following equivalent circuit: $L + R_s + (R//CPE)_{MF} + (R//CPE)_{LF} + (R//CPE)_{VLF}$ [27] (MF, LF and VLF correspond to Middle, Low and Very Low Frequency, respectively), where $L$ corresponds to the set-up inductance (around $10^{-6}$ H) [28] and $R_s$ is a series resistance. The capacitances values, given in Table 3, are of about $10^{-4}$–$10^{-3}$, $10^{-2}$ and $10^{1}\,F\,cm^{-2}$ for $(R//CPE)_{MF}$, $(R//CPE)_{LF}$ and $(R//CPE)_{VLF}$, respectively, which is in accordance with the values frequently reported [29–31]. The polarisation resistance ($R_p$) is the sum of $R_{MF}$, $R_{LF}$ and $R_{VLF}$. From this value, the area specific resistance (ASR) can be determined ($ASR = R_p \cdot S/2$, where $S$ is the cathode's surface and the factor 1/2 accounts for the fact that symmetrical cells are tested).

The samples A and B exhibit ASR values at 700 °C of 0.12 and $0.09\,\Omega\,cm^2$, respectively (Fig. 3). This allows us to get access to the measurement error, which is of $0.03\,\Omega\,cm^2$ at 700 °C.

### 3.4. Analyse of the design of experiments by the software Statgraphics®

Based on the 27 recorded values issued from the design of experiments (Table 1), the dependence of the $ASR_{(700\,°C)}$ on the different parameters (see Table 1) has been analysed by the software Statgraphics®. The influence of the sintering temperature ($T$) and duration ($t$), the number of layers ($n$), the coupled effects ($Tt$, $Tn$ and $tn$) and the quadratic effects ($T^2$, $t^2$ and $n^2$) on the $ASR_{(700\,°C)}$ value has been determined. A parameter is considered meaningless if the result of a Snedecor test is obtained with a probability greater than 5%. This value of 5 % corresponds to the standardized effect value 2.3 on the Pareto diagram (Fig. 4). Based on this criterion, it appears that the $ASR_{(700\,°C)}$ depends mainly on the sintering temperature ($T$ and $T^2$).

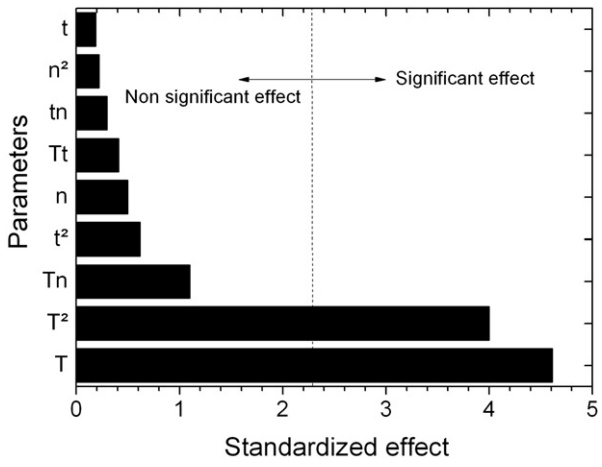


**Fig. 4.** Pareto diagram of the ASR.

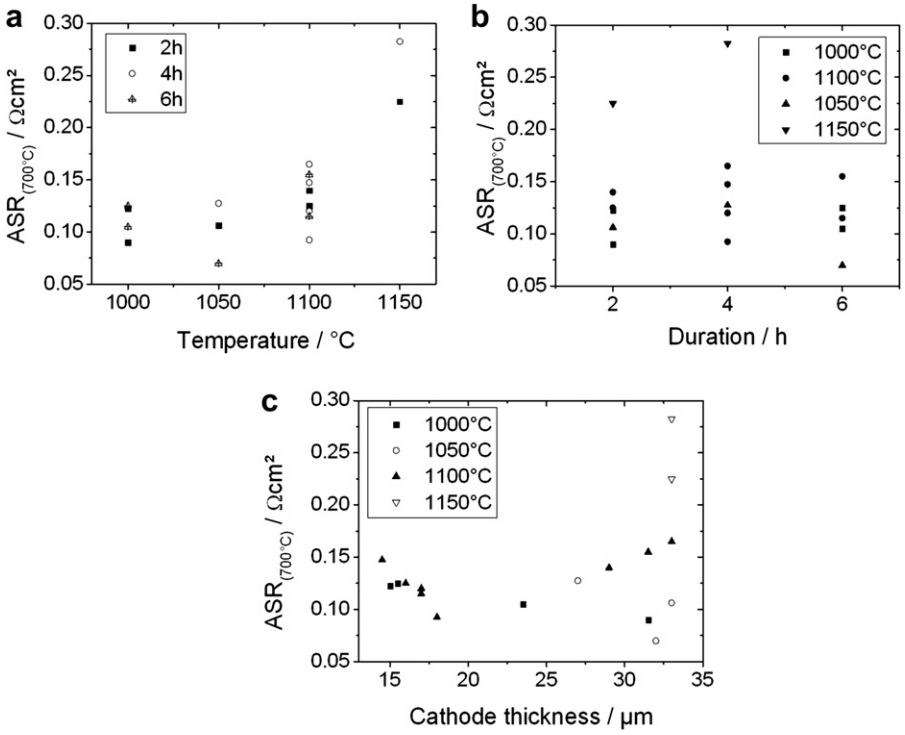


**Fig. 5.** $ASR_{(700\ ^\circ C)}$ evolution vs.: (a) the sintering temperature, (b) the sintering duration and (c) the cathode thickness.

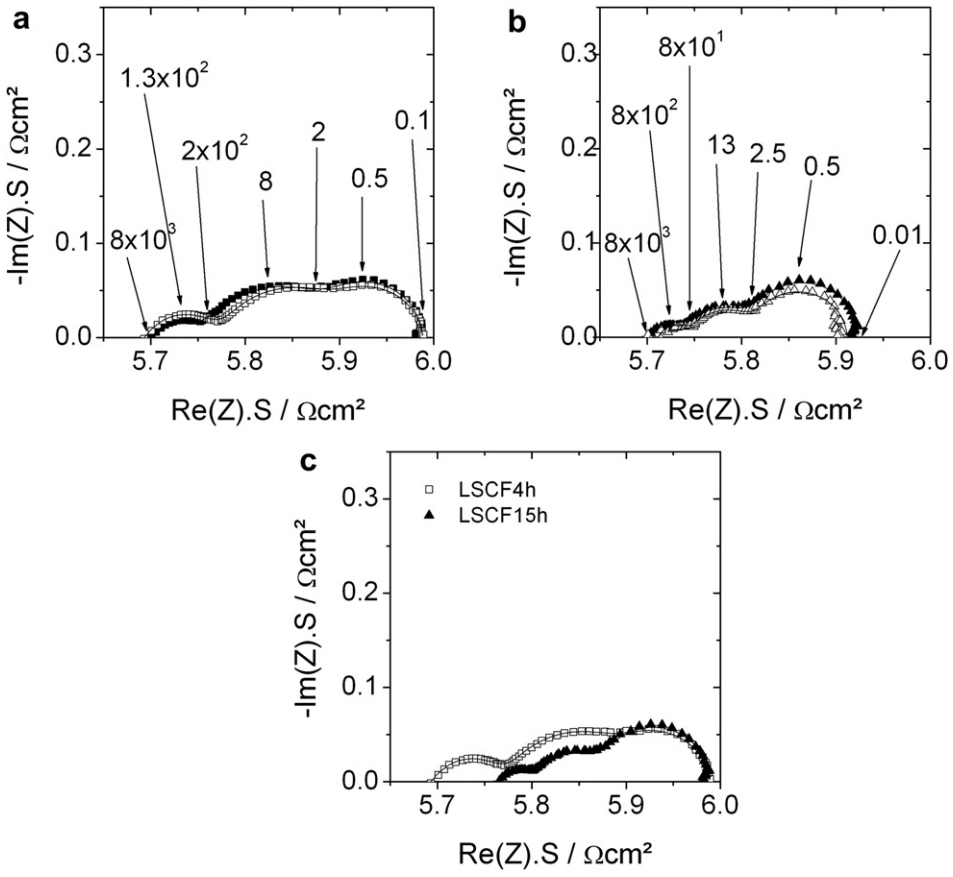


**Fig. 6.** Nyquist diagrams recorded at 700 °C with LSCF powder ball-milled for (a) 4 h and (b) 15 h and (c) superimposition of the diagrams obtained for the two grain sizes (LSCF powder ball-milled for 4 h □ and 15 h ▲). Frequencies are indicated in Hz. The lines correspond to the diagrams calculated with values gathered in Table 4.

**Table 4**
Comparison of resistance and capacity values determined from impedance diagrams 6a and 6b.

| Sample | $R_{MF}S$ ($\Omega\,cm^2$) | $C_{MF}/S$ ($F\,cm^{-2}$) | $R_{LF}S$ ($\Omega\,cm^2$) | $C_{LF}/S$ ($F\,cm^{-2}$) | $R_{VLF}S$ ($\Omega\,cm^2$) | $C_{VLF}/S$ ($F\,cm^{-2}$) |
|---|---|---|---|---|---|---|
| 6a-1 | 0.09 | $3\times10^{-4}$ | 0.12 | $2\times10^{-1}$ | 0.08 | 5 |
| 6a-2 | 0.13 | $10^{-4}$ | 0.09 | $2\times10^{-1}$ | 0.06 | 5 |
| 6b-1 | 0.07 | $5\times10^{-4}$ | 0.05 | $10^{-1}$ | 0.07 | 5 |
| 6b-2 | 0.05 | $10^{-3}$ | 0.07 | $2\times10^{-1}$ | 0.10 | 4 |

### 3.5. Influence of (T–t–n) on the $ASR_{(700\,^\circ C)}$ value

Fig. 5 presents the ASR evolution vs. (a) the sintering temperature and (b) duration and (c) the cathode thickness.

#### 3.5.1. Influence of the sintering temperature

Fig. 5(a) presents the ASR evolution vs. the sintering temperature for each sintering duration. The ASR value decreases drastically with temperature in the range 1050–1150 °C, to reach a minimum for sintering temperature around 1000–1050 °C.

#### 3.5.2. Influence of the sintering duration

According to the Pareto diagram of the ASR (Fig. 4), the sintering duration is the parameter that influences the least the cathode performance. Fig. 5(b) presents the ASR evolution vs. the sintering duration for each sintering temperature. No specific correlation between the sintering temperature and the ASR can be pointed out. However, as it was already seen on Fig. 5(a), all the ASR are comprised between 0.07 and 0.17 ($\pm0.03$) $\Omega\,cm^2$, except for the two samples sintered at 1150 °C ($ASR_{(700\,^\circ C)} = 0.23$ and $0.28\,\Omega\,cm^2$). This could be explained by the fact that using a too high sintering temperature (such as 1150 °C) leads to a loss of porosity and thus decreases the electrochemical performance.

#### 3.5.3. Influence of the thickness

In the statistical analyse of the results, the thickness was not taken into account because, on the contrary to the sintering temperature, the sintering duration and the number of layer, it isn't a first-order parameter, but a parameter that depends form the three earlier mentioned. However, it has been reported in the literature, that this parameter can have an influence on the cathode performance. Fig. 5(c) presents the ASR evolution vs. the cathode thickness for each sintering temperature. The smallest ASR value is observed for a sample with a thickness of 32 μm. However for the other samples, the ASR generally decreases as the cathode thickness increases up to 17–22 μm and then increases for larger thickness. Generally, the ASR decreases with the increase of the electrode thickness [29,32], however the trend we observed has already been reported with a composite LSM/YSZ cathode [33] (with a minimum around 40 μm).

As a conclusion it has been seen that the sintering temperature is the parameter that has the stronger effect on the cathode ASR at 700 °C and the best performance: $0.07\,\Omega\,cm^2$, has been obtained with a cathode of 32 μm sintered at 1050 °C for 6 h. This value competes with the best one reported in the literature [34].

### 3.6. Influence of the grain size on the $ASR_{(700\,^\circ C)}$ value

Previous conclusions have been obtained with LSCF powder ball-milled 4 h. As it has been shown in literature [35–37] that the powder grain size has an influence on the performance, this parameter will now be investigated. LSCF/BIT07/LSCF symmetrical cells ($n = 3$) have been realised with LSCF powder ball-milled for 4 and 15 h, and two samples have been realised with each powder. They have then been sintered ($T = 1050\,^\circ C$ and $t = 6$ h) and analysed by EIS and SEM.

For each tested grain size, the two diagrams, recorded at 700 °C, are superimposed (Fig. 6(a) and (b)), which confirms the reproducibility of both the design method and the measurement. The reproducibility can be quantified by comparing the corresponding resistance and capacitance values of the equivalent circuits, collected in Table 4. The error found here is of about $0.02\,\Omega\,cm^2$, which is very close to the one obtained in Section 3.3.2. ($0.03\,\Omega\,cm^2$). The results show a significant improvement of the

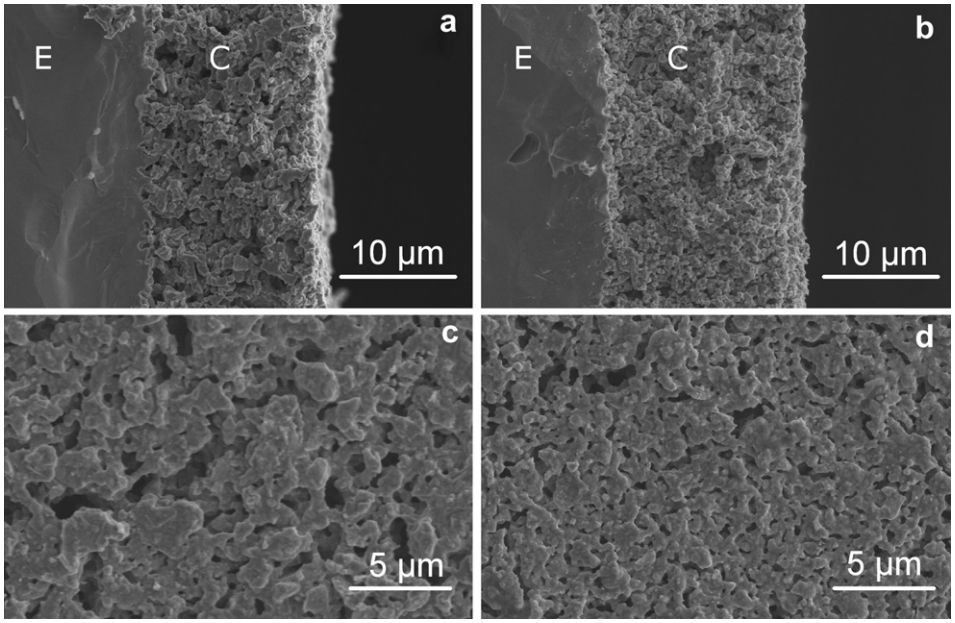


**Fig. 7.** SEM images of the fracture surface of the cathode/electrolyte and of the cathode surface after a sintering treatment of 6 h at 1050 °C, the cathode is made of LSCF powder ball-milled for: 4 h ((a) and (c)) and 15 h ((b) and (d)).

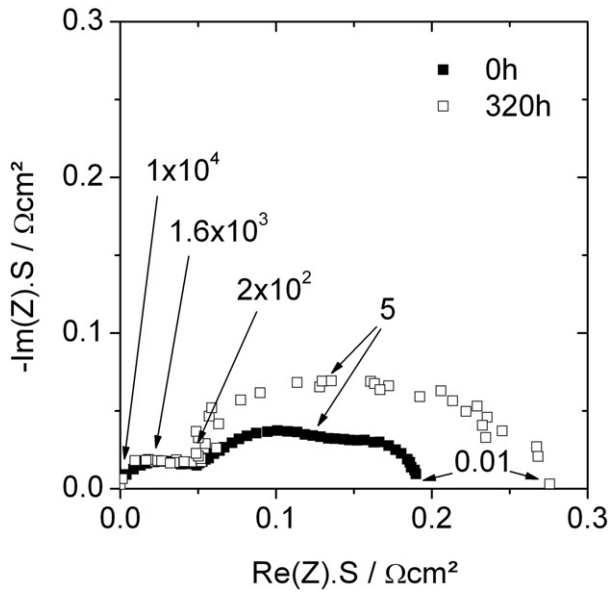


**Fig. 8.** Nyquist diagrams recorded at 700 °C before (■) and after (□) ageing experiment for the LSCF cathode b15-n4-T1050-t6. Frequencies are indicated in Hz.

ASR value at 700 °C when decreasing the cathode grain size: 0.15 and 0.1 Ω cm$^2$ for powders ball-milled 4 and 15 h, respectively.

The diagrams obtained for the two grain sizes have been shifted in order to merge the two low frequency intercepts with the real axis (Fig. 6(c)). It appears that the middle frequency (MF) and low frequency (LF) contributions are smaller for the cathode realised with the powder ball-milled for 15 h. Nevertheless the very low frequency (VLF) contribution is similar to the one observed with the powder ball-milled for 4 h, indicating that there is no improvement concerning the gas conduction through the electrode.

Fig. 7 presents the SEM images of the cathode/electrolyte interface and of the cathode surface for the two grain sizes. The cathode thicknesses are similar: 15 μm and 17 μm for the powders ball-milled for 4 and 15 h, respectively. The microstructure obtained with the powder ball-milled for 15 h seems finer and the porosity better distributed (Fig. 7(b) and (d)). In this case, for the same cathode thickness, as there is no significant change concerning the VLF contribution, the improvement of the electrochemical performance could be explained by the fact that the use of smaller particles increases the triple phase boundary length [38].

### 3.7. Ageing experiment

It has been demonstrated above that an LSCF cathode deposited on a BIT07 substrate exhibited good performance for a large range of both thermal treatments and cathode grain sizes. Thus the electrochemical performance evolution with time of a symmetrical cell, prepared with LSCF powder ball-milled 15 h ($b = 15$) with 4 deposited layers ($n = 4$) and sintered 6 h ($t = 6$) at 1050 °C; noted b15-n4-T1050-t6, has been followed by EIS during 320 h at the working temperature of 700 °C.

The $ASR_{(700\,°C)}$ before ageing (at $t = 0$ h) and after ageing (at $t = 320$ h) are of about 0.10 and 0.14 Ω cm$^2$, respectively. Those values correspond to an increase of 40% of the initial value and an average degradation rate of 0.125% h$^{-1}$. This value is in complete agreement with the one obtained previously [18] for an LSCF/BIT07 assembly (sintered for 12 h at 1150 °C), which presented an average degradation rate of 0.125 % h$^{-1}$ (an average increase of Rp of around 40 % has been recorded during 320 h of test).

Fig. 8 presents the Nyquist diagrams obtained at 700 °C before and after ageing. During the ageing experiment, a small variation of $R_s$ has been observed; it has been attributed to local changes at the interface resulting in a small variation of the electrolyte thickness. To compare the two diagrams more easily, their high frequency intercepts with the real axis have been reset at the origin.

The middle frequency contribution does not present any modification on the contrary to the low and the very low frequency contributions which increase with the time. This means that the degradation mechanisms are linked to the mass transfer phenomena (decrease of porosity and/or reduction of the dissociation or transportation rate of the $O_2$ or $O^{2-}$ species). However in this case, no obvious evolution of the microstructure has been observed after the ageing experiment and the cathode seems to present the same porosity as before the measurement.

I.M. Torres da Silva et al. have studied the degradation of an LSM/YSZ/LSM symmetrical cell at 650 °C for 156 h and have obtained the same result, with a modification of the Nyquist diagram appearing only for the frequencies below 10 Hz [39]. After 156 h the ASR has increased of 33% with a degradation rate of 0.22% h$^{-1}$, which is close to our value (0.125% h$^{-1}$). Although this value competes favourably with published ones, it is still too high and thus further investigations are now in progress.

## 4. Conclusion

LSCF ($La_{0.58}Sr_{0.4}Co_{0.2}Fe_{0.8}O_{3-\delta}$)/BIT07 ($BaIn_{0.3}Ti_{0.7}O_{2.85}$) cathode/electrolyte assemblies have been successfully prepared by screen-printing. The analysis of the cathode/electrolyte interface confirms the presence of an accommodating layer between the two compounds which seems to be composed of $Ba_xLa_{0.58(1-x)}Sr_{0.4(1-x)}In_{0.3x}Ti_{0.7x}Co_{0.2(1-x)}Fe_{0.8(1-x)}O_{3-\delta}$ (BLSITCFx) phases or of LSCF/BIT07, LSCF/BLSITCFx or BLSITCFx/BIT07 composites, or even of mixtures of all these compounds.

Symmetrical cells LSCF/BIT07/LSCF have been prepared and the optimisation of the cathode design (thermal treatment, grain size, cathode thickness) has been realised thanks to electrochemical impedance spectroscopy: an ASR value of 0.07 Ω cm$^2$ at 700 °C has been finally obtained. This study has also shown that, for a large range of thermal treatments, cathode grain sizes and thicknesses, most of the cathodes exhibit good performance (below 0.2 Ω cm$^2$).

The ageing of a cathode/electrolyte/cathode assembly has been followed by EIS and it appears that its performance decrease with the time at the working temperature. The evolution of the Nyquist diagram upon ageing suggests a modification of the adsorption or dissociation rate or/and of the gas diffusion. To determine the cause of the degradation, morphological and chemical characterisations still have to be carried out.

Based on this study, the realisation of complete anode/BIT07/LSCF cells has been realised and complete cell test have been performed [40].

## References

[1] B.C.H. Steele, Nature 400 (1999) 619–621.
[2] E. Evers-Tiffee, A. Weber, D. Herbstritt, J. Eur. Ceram. Soc. 21 (2001) 1805–1811.
[3] F. Tietz, V.A.C. Haanappel, A. Mai, J. Mertens, D. Stöver, J. Power Sources 156 (2006) 20–22.
[4] S. Uhlenbruck, T. Moskalewicz, N. Jordan, H.-J. Penkalla, H.P. Buchkremer, Solid State Ionics 180 (2009) 418–423.
[5] A. Mai, M. Becker, W. Assenmacher, F. Tietz, D. Hathiramani, E. Ivers-Tiffée, D. Stöver, W. Mader, Solid State Ionics 177 (2006) 1965–1968.
[6] J. Chen, F. Liang, S. Jiang, B. Chi, J. Pu, J. Li, J. Power Sources 183 (2008) 586–589.
[7] F. Qiang, K. Sun, N. Zhang, X. Zhu, S. Le, D. Zhou, J. Power Sources 168 (2007) 338–345.
[8] J. Chen, F. Liang, B. Chi, S.P. Jiang, L. Jian, J. Power Sources 194 (2009) 275–280.

[9] Y. Lin, S.A. Barnett, Solid State Ionics 179 (2008) 420–427.
[10] S. Lee, H. Song, S. Hyun, J. Kim, J. Moon, J. Power Sources 187 (2009) 74–79.
[11] C. Torres-Garibay, D. Kovar, A. Manthiram, J. Power Sources 187 (2009) 480–486.
[12] D. Beckel, A. Dubach, A. Grundy, A. Infortuna, L. Gauckler, J. Eur. Ceram. Soc. 28 (2008) 49–60.
[13] R.S. Joshi, R.K. Nimat, S.H. Pawar, J. Alloys Compd. 471 (2009) 461–465.
[14] J. Soo Ahn, S. Omar, H. Yoon, J.C. Nino, E.D. Wachsman, J. Power Sources 195 (2010) 2131–2135.
[15] Z. Gao, J. Huang, Z. Mao, C. Wang, Z. Liu, Int. J. Hydrogen Energy 35 (2010) 731–737.
[16] D. Prakash, T. Delahaye, O. Joubert, M.-T. Caldes, Y. Piffard, J. Power Sources 167 (2007) 111–117.
[17] M. Letilly, A. Le Gal La Salle, M. Marrony, O. Joubert, Fuel Cells 9 (2009) 622–629.
[18] M. Letilly, A. Le Gal La Salle, A. Lachgar, O. Joubert, J. Power Sources 195 (2010) 4779–4784.
[19] S.B. Adler, Chem. Rev. 104 (2004) 4791–4844.
[20] L. Baqué, E. Djurado, C. Rossignol, D. Marinha, A. Caneiro, A. Serquis, ECS Trans. 25 (2009) 2473–2480.
[21] M. Letilly, O. Joubert, M.T. Caldes, A. Le Gal La Salle, Int. J. Hydrogen Energy 30 (2012) 4346–4355.
[22] T. Delahaye, O. Joubert, M.-T. Caldes, Y. Piffard, P. Stevens, Solid State Ionics 177 (2006) 2945–2950.
[23] J.M. Ralph, C. Rossignol, R. Kumar, J. Electrochem. Soc. 150 (2003) A1518–A1522.
[24] Q.-A. Huang, R. Hui, B. Wang, J. Zhang, Electrochim. Acta 52 (2007) 8144–8164.
[25] A. Le Gal La Salle, M. Letilly, E. Quarez, M. Caldes, O. Joubert, J. Power Sources 196 (2011) 10576–10583.
[26] D. Johnson, ZView: A Software Program for IES Analysis Version 2.8, Scribner Associates, Inc, Southern Pines, NC, 2002.
[27] J.-D. Kim, G.-D. Kim, J.-W. Moon, Y.-i. Park, W.-H. Lee, K. Kobayashi, M. Nagai, C.-E. Kim, Solid State Ionics 143 (2001) 379–389.
[28] D. Marrero-López, J. Peña-Martínez, J.C. Ruiz-Morales, M. Gabás, P. Núñez, M.A.G. Aranda, J.R. Ramos-Barrado, Solid State Ionics 180 (2010) 1672–1682.
[29] V. Dusastre, J.A. Kilner, Solid State Ionics 126 (1999) 163–174.
[30] F.S. Baumann, J. Fleig, H.-U. Habermeier, J. Maier, Solid State Ionics 177 (2006) 1071–1081.
[31] M. Shah, S. Barnett, Solid State Ionics 179 (2008) 2059–2064.
[32] X.J. Chen, S.H. Chan, K.A. Khor, Electrochim. Acta 49 (2004) 1851–1861.
[33] A. Barbucci, M. Carpanese, A. Reverberi, G. Cerisola, M. Blanes, P. Cabot, M. Viviani, A. Bertei, C. Nicolella, J. Appl. Electrochem. 38 (2008) 939–945.
[34] L. Baqué, A. Caneiro, M.S. Moreno, A. Serquis, Electrochem. Commun. 10 (2008) 1905–1908.
[35] K. Sasaki, J.-P. Wurth, R. Gschwend, M. Gödickemeier, L.J. Gauckler, J. Electrochem. Soc. 143 (1996) 530–543.
[36] J. Mertens, V.A.C. Haanappel, C. Wedershoven, H.-P. Buchkremer, J. Fuel Cell Sci. Technol. 3 (2006) 415–421.
[37] F. Tietz, A. Mai, D. Stöver, Solid State Ionics 179 (2008) 1509–1515.
[38] J. Liu, A.C. Co, S. Paulson, V.I. Birss, Solid State Ionics 177 (2006) 377–387.
[39] I.M. Torres da Silva, J. Nielsen, J. Hjelm, M. Mogensen, ECS Trans. 25 (2009) 489–498.
[40] M. Letilly, O. Joubert, A. Le Gal La Salle, J. Power Sources 206 (2012) 210–214.